Lie groups, Space-Variant Fourier Analysis and the Exponential Chirp Transform *

Giorgio Bonmassar

Dept. Biomedical Engineering
Boston University
Boston, MA 02146
e-mail: giorgio@bu.edu

Eric L. Schwartz

Dept. Cognitive and Neural Systems
Boston University
Boston, MA 02146
e-mail: eric@thing4.bu.edu

Abstract

The use of visual representations in which retinal neurons receptive fields are not constant over the visual field is universal in the visual systems of higher vertebrates, and is coming to play an important role in active vision applications. The breaking of translation symmetry that is unavoidably associated with non-uniform sampling presents a major algorithmic complication for image processing. In this paper we use a Lie group approach to derive a kernel which provides a quasi-shift (i.e. approximate shift) invariant template matching capability, under normal convolution in the distorted (range) coordinates of the non-uniform mapping. We work out the special case of the log-polar mapping, which is of great interest in vision; in this case, we call the associated linear integral transform the "exponential chirp transform" (ECT). The method is, however, general for other forms of mapping, or warp, function.

1 Introduction

This paper addresses a fundamental difficulty in performing frequency domain image processing on image architectures which are strongly space-variant, and, in particular, which are described by the log-polar map, or one of its variants. The term space-variant denotes the cascade of a an anti-aliasing non-isotropic filter (see [24]) and a non-uniform sampling stage. The log-polar map is of interest in computer vision for two major reasons:

1. It has been shown to be a good approximation to the image format used in primate and human visual cortex [21], and would seem to provide advantages to machine vision which are similar to those that are already understood to apply to human vision.

2. It provides a continuum model for variable resolution, or foveating pyramid architectures in machine vision.

*Work supported by ARPA ANNT-ONR N00014-92-C-0119 and ONR MURI N60014-95-I-0409.

Recently, a number of research groups have constructed machine vision systems based on this architecture [26, 1, 3, 11, 17, 2].

The specific problem addressed in this paper is the use of Lie Group methods to formulate and then solve a specific partial differential equation (PDE). The solution of this PDE yields a space-variant kernel which provides a shift-invariant property analogous to that of the conventional Fourier transform for image architectures which are space-variant. This seemingly contradictory result is expected to be of fundamental importance to image processing in space-variant applications. Using the kernel that we have derived, which we call the exponential chirp kernel (ECT), it is possible to convolve an image in, for example, log-polar coordinate form, and yet retain the advantageous shift invariances associated with conventional Fourier Analysis. We have also derived, in other work, a fast algorithm for this convolution [4]. This work, together with the natural data compression provided by space-variant architectures, allows extremely high-speed template matching (which we estimate at 50-100 convolutions/second) to be performed with a single low-cost DSP chip. We show some examples of template matching, using this methodology, in the present paper.

The log-polar (or more accurately, complex logarithmic) map is defined as follows (eq.(11) expresses the mapping in terms of real coordinates):

$$w = K \log(z + a) \tag{1}$$

In this equation, K is an experimental constant which is only of relevance to the biological scale factor of a particular map, and will be dropped in the following discussion (see [21] for a review of estimates of this parameter), "a" a real constant [15] that deals with the singularity at the origin, complex "z" represents visual pixel coordinates, and complex "w" represents log-polar coordinates. In the context of computer graphics, the log-polar coordinate transform must be adjoined to an algorithm for image warping, which expresses the space-variance of pixel size, as well as

pixel location. This can be stated as follows: we associate each pixel W from the range of the log-polar warp a set of domain pixels $f^{-1}(W)\epsilon Z$, where Z represents the set of domain pixels which would come, commonly, from a conventional t.v. image. Formally, using the notation χz to represent the location of a domain pixel,

$$f^{-1}(W) = Z \mid \log(\chi z + a)\,\epsilon W \qquad (2)$$

Thus, each pixel W represents the support of a small group of pixels in the domain, whose size increases with increasing distance from the origin. The location of these pixels is expressed by the complex logarithmic coordinate change of eq.(1).

Figure 1 shows a conventional video frame, with a central fixation point.

Figure 2 shows a log polar mapping of Figure 1.

The log image has 4096 pixels, while the source image has 65536, yielding a compression of more than one order of magnitude[1]. Given the ability to point the sensor (i.e. active vision), and appropriate attentional algorithms to determine where to move the sensor, it is clear that this architecture could be extremely useful. Yet, the size and the "shape" of image features changes radically as the "fixation" point is moved, as is evident in the figure. In other words, the good news of SV vision is that enormous reductions in space-complexity can be achieved. The bad news is that even the simplest image processing tasks can become extremely difficult.

Historically, there have been three approaches to this problem. First, one might work in the inverse mapped log-polar image. But, the number of pixels in this image is equal to that of Figure 1 (when represented in a device or memory with conventional constant pixel architecture), therefore sacrificing one of the principle motivations of the method. Second, one might precede the log-polar mapping with a Fourier transform, i.e. use a Mellin-Fourier transform, as has been pointed out during the past three decades, e.g. [5, 8, 19, 23]. Third, one may use the connectivity graph of the transformed domain [25]. This approach cannot be generalized for frequency domain applications. The Mellin-Fourier transform is equivalent to applying the operations of Fourier transform, log polar mapping and Fourier transform to the original image. The first Fourier transform is, up to a phase, translation invariant. The log-polar transform provides size and rotation invariance, up to a spatial shift (see [19]) and the final Fourier transform reduces this shift to a phase. The Mellin transform has generated a fair amount of attention as an example of a geometrically invariant linear integral transform method.

At this point, it is important to point-out a fact which has not always been emphasized. Although the Mellin transform technique does solve the problem of working in a space-variant domain such as the log-polar map, it does so, by, in a sense, "throwing the baby out with the bath water." The initial Fourier transform, which nullifies the unpleasant space-variance of the log-polar map, also removes one of the the main advantages for which the log-polar map was introduced (see [20, 10]). The log-polar mapping used in the Mellin transform is in frequency space, and thus, rather than having a "foveating" or space-variant vision architecture, the Mellin transform provides a "fovea" in frequency space. The practical disadvantage of this is that it requires two dimensional (FFT) transform of the full rank image. This is computationally unfavorable for many real-time vision applications, and obviates the space-complexity advantages outlined above for the log-polar mapping.

In the present paper, we derive, using Lie Group methods, the exponential chirp transform (ECT), which retains the favorable translation symmetry of the Mellin-Fourier approach, but does not require a transformation back into the original image plane. As outlined in eq.(2), we seek a form of space-variant kernel, which, when convolved with a space-variant image such as produced by the log-polar map, provides an analogue of the usual shift property that the Fourier transform have in conventional space-invariant imaging. Specifically, we wish our kernel to have the property that convolution with the image (in the range coordinate system of the warped image) changes only by a phase when a shift is applied in the **domain** coordinates. Such a kernel would allow us to generalize Fourier Analysis to space-variant mappings, and would allow an efficient computation of the convolution, since our range coordinate system has a very small number of pixels. We will now provide a brief review of Lie Group methods in partial differential equations, and we will then show a PDE system whose solution is the desired kernel. This method may be used in general to set up the PDE system which solves this problem for an arbitrary space-variant mapping. Then, we will demonstrate a solution to this PDE system for the particular case of the log-polar map. Finally, we show several examples in which we have applied template matching in a simple optical character recognition demonstration using this methodology, illustrating shift invariant template matching, performed with high efficiency in the log-polar image format.

2 Lie Group Theory

Consider the following invertible coordinate transformation in a two-dimensional space:

$$(\hat{x}, \hat{y}) = (\phi(x, y, \rho), \psi(x, y, \rho)) \qquad (3)$$

If eq.(3) is a smooth one-dimensional manifold (e.g. curve parameterized by ρ) with smooth inverse map, such that:

$$(\phi(\hat{x}, \hat{y}, \rho_1), \psi(\hat{x}, \hat{y}, \rho_1)) = (\phi(x, y, \rho_2), \psi(x, y, \rho_2)) \qquad (4)$$

where ρ_1 and ρ_2 are two parameters, then eq.(3) represents a one-parameter Lie group, parameterized by ρ;

[1] for human vision the compression is 4 orders of magnitude [15].

ρ_0 identifies the identity element (i.e. identity transformation):

$$(x, y) = (\phi(x, y, \rho_0), \psi(x, y, \rho_0)) \tag{5}$$

We can express the coordinate transformation using the following Taylor's series, expanded at ρ_0:

$$\begin{gathered}(\hat{x}, \hat{y}) = (x, y) + \\ (\alpha(x, y), \beta(x, y))\,[\rho - \rho_0] + \mathbf{o}([\rho - \rho_0]^2)\end{gathered} \tag{6}$$

where

$$\begin{aligned}\alpha(x, y) &= \frac{\partial \phi(x, y, \rho)}{\partial \rho}\,|_{\rho=\rho_0} \\ \beta(x, y) &= \frac{\partial \psi(x, y, \rho)}{\partial \rho}\,|_{\rho=\rho_0}\end{aligned} \tag{7}$$

The *infinitesimal generator* [13] of the Lie Group:

$$\mathbf{g} = \alpha(x, y)\frac{\partial}{\partial x} + \beta(x, y)\frac{\partial}{\partial y} \tag{8}$$

generates a one-parameter group by direct solution of the differential equation expressed in eq.(7), taking eq.(5) as initial conditions. The elements of a Lie group may be also computed by the exponential map (see [14]): $\exp(\rho\mathbf{g})(x, y)$.

Particular attention has to be placed on the group's parameter, because it generates the generic element of the Lie group. In particular eq.(5) can be rewritten in this notation, where $\rho = 0$ determinates the identity element of the group:

$$\exp(0\,\mathbf{g})(x, y) = (x, y) \tag{9}$$

The infinitesimal generator $\mathbf{g}$ is:

$$\left.\frac{d}{d\rho}\right|_{\rho=0} [\exp(\rho\mathbf{g})(x, y)] = \mathbf{g}\,|_{(x,y)} \tag{10}$$

Example 1 The generator $\mathbf{g_t} = \frac{\partial}{\partial x}$ generates the group of the x-axis translations:

$$(\hat{x}, \hat{y}) = (x + \rho, y)$$

Example 2 Considering the group of rotations in the plane:

$$(\hat{x}, \hat{y}) = (x\,\cos(\rho) - y\,\sin(\rho), x\,\sin(\rho) + y\,\cos(\rho))$$

according to eq.(7)

$$\alpha(x, y) = \frac{\partial \phi(x, y, \rho)}{\partial \rho}\,|_{\rho=0} = -y$$

$$\beta(x, y) = \frac{\partial \psi(x, y, \rho)}{\partial \rho}\,|_{\rho=0} = x$$

we obtain the infinitesimal generator $\mathbf{g_r}(x, y) = -y\,\frac{\partial}{\partial x} + x\,\frac{\partial}{\partial y}$

Example 3 The generator $\mathbf{g_d} = x\,\frac{\partial}{\partial x} + y\,\frac{\partial}{\partial y}$, using eq.(7) we obtain the following system of ordinary differential equations,

$$\begin{aligned}\frac{\partial x}{\partial \rho} &= x \\ \frac{\partial y}{\partial \rho} &= y\end{aligned}$$

which generates the group $(e^\rho\,x, e^\rho\,y)$ of exponential scalings.

3 The Exponential Chirp Transform (ECT)

We consider here the following two-dimensional log-polar (or complex logarithmic) transformation which is appropriate to model primate visual cortex [15]: $w = \log(z + a)$, where "a" is a definite positive parameter. [2] The transformation between spaces can therefore be written:

$$\begin{aligned}\xi &= \log\sqrt{(x + a)^2 + y^2} \\ \eta &= \arctan\frac{y}{x + a}\end{aligned} \tag{11}$$

Our goal is to achieve "shift-invariance", like that of the usual Fourier transform, in the log-polar plane. Thus given an image $s(\xi, \eta)$ in the domain of the polar-log mapping , we require a change of variables $(\xi, \eta) \rightarrow (f(\xi, \eta), g(\xi, \eta))$ so that translations in the original plane (x, y) will result only in phase factors for the following Fourier transform:

$$\begin{aligned}\iint_{\mathcal{D}} s(\xi, \eta)\,|J(\xi, \eta)|\,\exp[-2\,\pi\,j(f(\xi, \eta)\,k + \\ g(\xi, \eta)\,h)]\,d\xi\,d\eta\end{aligned} \tag{12}$$

where $|J(\xi, \eta)|$ is the determinant of the Jacobian of the transformation and $\mathcal{D} \equiv \{(\xi, \eta) : -\infty \leq \xi < +\infty$ and $-\frac{3}{2}\pi \leq \eta \leq \frac{\pi}{2}\}$. The following Lie group will enable us to find the two functions $(f(\xi, \eta)$ and $g(\xi, \eta))$

[2] The complex log transformation requires a branch cut, which is taken in this case to divide the plane into two parts ($Real(z) > 0$ and $Real(z) < 0$. Note that this is identical to (and in fact was motivated by) the anatomy of the brain: the two sides of this mapping are in direct correspondence with the two hemispheres of the brain. The visual cortex, which is of the form of a complex logarithmic mapping, is divided in this way for similar reasons. See [21] for discussion of the biological evidence for log-polar mapping in primate visual cortex.

by solving a set of partial differential equations (PDE). These equations identify the group of symmetries with respect to simple translations in space. This analysis follows that of [12, 16].

A generic infinitesimal generator under a change of coordinates ($x = \phi(\xi,\eta), y = \psi(\xi,\eta)$) and inverse transformation ($\xi = \phi^{-1}(x,y), \eta = \psi^{-1}(x,y)$), has the form,

$$\begin{aligned}\mathbf{g} = &\left(\alpha(x,y)\frac{\partial\phi^{-1}(x,y)}{\partial x}+\right.\\ &\left.\beta(x,y)\frac{\partial\phi^{-1}(x,y)}{\partial y}\right)\Big|_{(x=\phi(\xi.\eta),y=\psi(\xi,\eta))}\frac{\partial}{\partial\xi}+\\ &\left(\alpha(x,y)\frac{\partial\psi^{-1}(x,y)}{\partial x}+\right.\\ &\left.\beta(x,y)\frac{\partial\psi^{-1}(x,y)}{\partial y}\right)\Big|_{(x=\phi(\xi.\eta),y=\psi(\xi,\eta))}\frac{\partial}{\partial\eta}\end{aligned} \tag{13}$$

where $\alpha(x,y)$ and $\beta(x,y)$ are the same as in eq.(8). The horizontal shift infinitesimal generator (see example 1), under the log-map transformation is therefore,

$$\mathbf{g_t} = \exp(-\xi)\cos(\eta)\frac{\partial}{\partial\xi} - \exp(-\xi)\sin(\eta)\frac{\partial}{\partial\eta} \tag{14}$$

Using eq.(13) the infinitesimal generator for rotation (see example 2) is $\frac{\partial}{\partial\eta}$ and for exponential scaling is $\frac{\partial}{\partial\xi}$. The log-map transformation, therefore, changes the group of exponential scalings and rotations into a group of simple horizontal and vertical translations. [3] We are interested in "f" and "g" which satisfies the following system of partial differential equations, expressed by knowing that the generator of translations in $\Re^2$ is the vector $(1,0)$ (see example 1) [4]),

$$\exp(-\xi)\cos(\eta)\frac{\partial f(\xi,\eta)}{\partial\xi} - \exp(-\xi)\sin(\eta)\frac{\partial f(\xi,\eta)}{\partial\eta} = 1$$

$$\exp(-\xi)\cos(\eta)\frac{\partial g(\xi,\eta)}{\partial\xi} - \exp(-\xi)\sin(\eta)\frac{\partial g(\xi,\eta)}{\partial\eta} = 0$$

It can be verified by direct substitution that the PDE above has a (particular) solution:

$$\begin{aligned}f(\xi,\eta) &= \exp(\xi)\cos(\eta) - a\\ g(\xi,\eta) &= \exp(\xi)\sin(\eta)\end{aligned} \tag{15}$$

The final result of this analysis is to write the explicit form of the exponential chirp transform (ECT), by combining eq.(15) and eq.(12),

$$\begin{aligned}\iint_{\mathcal{D}} s(\xi,\eta)\exp(2\xi)\exp[-2\pi j[k\,(\exp(\xi)\cos(\eta)\\ - a) + l\,\exp(\xi)\sin(\eta)]\,d\xi\,d\eta\end{aligned} \tag{16}$$

where $\mathcal{D} \equiv \{(\xi,\eta) : -\infty \le \xi < +\infty \text{ and } -\frac{3}{2}\pi \le \eta \le \frac{\pi}{2}\}$.

The ECT has the following properties:

1. Shift in the domain causes only a phase change in part of the complex exponential chirp transform[5]. This transform is done by using the exponential chirp kernel and the warped image (i.e. the image in the range coordinates) as in eq.(16).

2. This result may be extended to arbitrary mappings, by setting up the corresponding PDE, and solving it. In the present case, we have derived it for the class of log-polar mappings of the form $\log(z + a)$.

3. This mapping is correctly "foveating", i.e. space-variant, unlike the Mellin transform. It thus allows us to exploit the efficiency of computing in the typically small image sizes that result from space-variant imaging systems.

4 Results

We will now show some practical examples of application of the ECT, with the use of real images of tools. Working in a distorted space, or in particular coping with a non-uniform sampling, requires special care in order to avoid aliasing. Basically both kernel and image have to be filtered before the actual integral transformation so that both would satisfy Shannon's sampling theorem. Regions near the fovea which are sampled with a higher sampling frequency require a less abrupt band-pass filtering than regions in the periphery which are sampled much more coarsely. Aliasing is avoided when the image is filtered with a position-dependent band-pass filter before sampling. The images of tools in Figure 1 form an array of 256 by 256; the fovea is always centered in the center of the image with $R = 128$; the log-map images are 64 by 64 with parameter $a = 1.0$; therefore the polar log-map introduces a compression factor of 16. The tools image was initially filtered with an anti-aliasing non-uniform mean-filter. The image was divided into sectors with

[3] It is important to note here that size and rotation symmetry is provided by the map $log(z+a)$ only in the limit that $a = 0$. Realistic models of primate anatomy require a small but finite a, so provide size and rotation scaling at regions larger than this value of a.

[4] It does not really matter if we use the vector $(1,0)$ or $(0,1)$, it will only differ by a transposition of the ECT matrix.

[5] It is important to note that due to the space-variant (i.e. non-isotropic filtering followed by a non-uniform sampling) nature of the architecture, two shifted objects, one centered in the fovea and one shifted in the periphery, have, in general, different frequency representations. When proper non-isotropic filtering and non-uniform sampling is introduced (see [4]), a low frequency band is approx. common to both objects and in this band the phase change is detectable.

Figure 1: An image of tools uniformly sampled.

Figure 2: The log-polar representation of the image of tools.

exponentially growing radius, and the polar-log representation was given by taking the average value in every sector, as shown in Figure 2
The kernel of the ECT, in eq.(16), is clearly a complex function in which the frequency of the real and imaginary part grow exponentially with ξ. Therefore the kernel must be windowed to zero (on the (ξ, η) plane) when it reaches too high frequency according to the sampling used. This can be done using an ideal filter or by using one of the common windows (e.g. Bartlett, Hamming, Blackman, etc.), but in our examples we used ideal filters. The results in figures 3 and 4 show that the ECT is capable of locating a shifted copy of a tool, even in the presence of another object in the scene. A special phase-only filter is used as a matching algorithm (see [4]). All computations are performed in log-polar coordinates.

5 Conclusions

In the present paper, we have shown the solution of how to combine the space-variant imaging properties of a mapping, such as the complex logarithm, which plays a major role both in biological vision and in real-time active vision applications, with the properties of the Fourier transform. We have used Lie Group methods to set up a partial differential equation whose solution is the kernel which gives us the desired invariance properties, in the range coordinates of the image warp. In other work, [4], we have developed a highly optimized algorithm that allows computation of the ECT with complexity $O(N^2 \log(N))$ (i.e. the same as the FFT). From the point of view of real-time vision, this allows us to combine the space-efficiency of the log-polar mapping with the convenience of frequency domain template matching and image processing. We

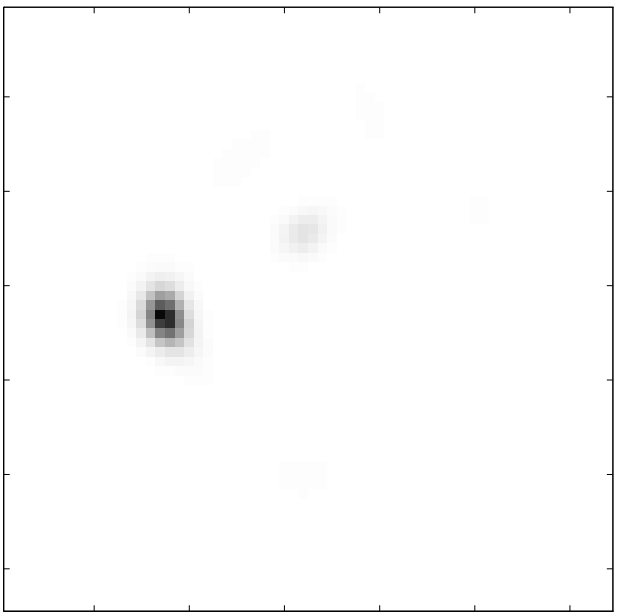

Figure 3: Result of matching the screwdriver template, using the exponential chirp transform together with a phase only filter, the matching is done in the usual uniform sampled plane.

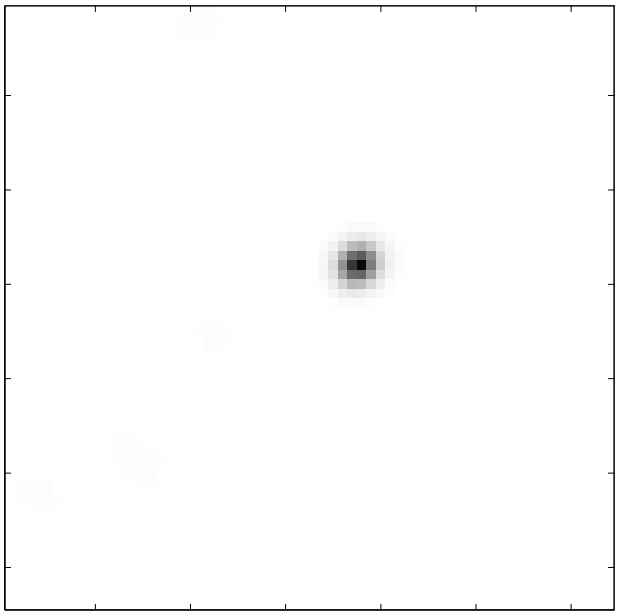

Figure 4: Result of matching the scissor template using the exponential chirp transform together with a phase only filter, in the original image domain.

have estimated that the ECT can be performed at about 50-100 transforms/second, using a single DSP processor (e.g. TI320C40). This provides the possibility of performing shift, size and rotation[6] invariant template matching in low-cost machine vision systems at rates which are comparable to optically based template matching! The practical importance of this work is threefold:

- A Space-Variant Generalization of the Mellin transform is described, which allows efficient image processing operations to be computed on log-polar image formats. This provides, for the first time, a possible reconciliation of the strongly space-variant nature of biological vision with the properties of global Fourier analysis.
- Lie Group methods are outlined which provide a method of generalizing this result to arbitrary space-variant mappings.
- The difficulty of performing efficient image processing operations on space-variant image architectures is solved.

6 Acknowledgment

The authors thank Prof. Alexander V. Levichev for reading, criticizing and suggesting many improvements on the manuscript.

[6]Size and rotation invariance is achieved with the ECT by using a log-map in frequency (see [4]), so that changes in size or in rotation correspond to shifts in the ECT domain. Therefore we can infer the size and rotation of an object with respect to its template by performing template matching directly in the domain of the ECT.

References

[1] Baloch, A. A. and Waxman, A. M. (1991). Visual learning: adaptive expections, and behavioral conditioning of the mobile robot mavin. *Neural Networks*, 4:271–302.

[2] Baron, T., Levine, M. D., Hayward, V., and nand D. Grant, M. B. (1995). A biologically motivated robot eye system. *Proc. of the 8th Canadian Aeronautics and Space Institute Conference on Astronautics, Ottawa, Ontario.*, 8:231–240.

[3] Bederson, B., Wallace, R. S., and Schwartz, E. L. (1992). A miniaturized active vision system. In *11th IAPR International Conference on Pattern Recognition*, volume B of *Specialty Conference on Pattern Recognition Hardware Architecture*, pages 58–62, The Hague, Netherlands.

[4] Bonmassar, G. and Schwartz, E. (1995). Space-variant Fourier analysis: The exponential chirp transform. *IEEE Pattern Analysis and Machine Vision*, Submitted.

[5] Brousil, J. K. and Smith, D. R. (1967). Threshold logic network for shape invariance. *IEEE transactions on electronic computers*, EC-16(6):818–828.

[6] Burt, P. and Adelson, T. (1981). A Laplacian pyramid for data compression. *IEEE Transactions on Communications*, 8:1230–1245.

[7] Burt, P. J. (1988). Smart sensing within a pyramid machine. *IEEE Proceedings*, 76(8):1006–1015.

[8] Casasent, D. and Psaltis, D. (1976). Position, rotation and scale-invariant optical correlation. *Applied Optics*, 15:1793–1799.

[9] Cavanagh, P. (1978). Size and position invariance in the visual system. *Perception*, 7:167–177.

[10] Cavanagh, P. (1982). Functional size invariance is not provided by the cortical magnification factor *Vision Research*, 22:1409–1412.

[11] Engel, G., Greve, D., Lubin, J., and Schwartz, E. (1994). Space-variant active vision and visually guided robotics: Design and construction of a high-performance miniature vehicle. In *ICPR Proceedings*, ICPR-12, pages 487–490. International Conference on Pattern Recognition.

[12] Ferraro, M. and Caelli, T. M. (1988). Relationship between integral transform invariances and lie group theory. *J. Opt. Soc. Am. A*, 5(5):738–742.

[13] Ibragimov, N. H., editor (1994). *CRC handbook of Lie Group analysis of differential equations*, volume 1. CRC Press, Inc.

[14] Olver, P. J. (1993). *Applications of Lie groups to differential equations*. Springer-Verlag.

[15] Rojer, A. S. and Schwartz, E. L. (1990). Design considerations for a space-variant visual sensor with complex-logarithmic geometry. *10th International Conference on Pattern Recognition, Vol. 2*, pages 278–285.

[16] Rubinstein, J., Segman, J., and Zeevi, Y. (1991). Recognition of distorted patterns by invariance kernels. *Pattern Recognition*, 24(10):959–967.

[17] Sandini, G. and Dario, P. (1989). Active vision based on space-variant sensing. *Intl. Symp. on Robotics Research.*

[18] Schutz, B. F. (1980). *Geometrical Methods of Mathematical Physics.* Cambridge University Press.

[19] Schwartz, E. L. (1977). Spatial mapping in primate sensory projection: analytic structure and relevance to perception. *Biological Cybernetics*, 25:181–194.

[20] Schwartz, E. L. (1981). Cortical anatomy, size invariance, and spatial frequency analysis. *Perception*, 10:455–468.

[21] Schwartz, E. L. (1994). Computational studies of the spatial architecture of primate visual cortex: Columns, maps, and protomaps. In Peters, A. and Rocklund, K., editors, *Primary Visual Cortex in Primates*, volume 10 of *Cerebral Cortex.* Plenum Press.

[22] Schwartz, E. L., Greve, D., and Bonmassar, G. (1995). Space-variant active vision: Definition, overview and examples. *Neural Networks*, 8:1297–1308.

[23] Sheng and Arsenault (1986). Experiments on pattern recognition using invariant Fourier-Mellin descriptors. *J. Opt. Soc. Am. A*, 3(6):771–776.

[24] Thibos, L. N. and Bradley, A. (1995). Modelling off-axis vision II: the effect of spatial filtering and sampling by retinal neurons. In Peli, E., editor, *Vision models for target detection and recognition*, pages 338–379. World scientific.

[25] Wallace, R., Ong, P.-W., Bederson, B., and Schwartz, E. (1994). Space variant image processing. *International Journal of Machine Vision*, 13(1):In press.

[26] Weiman, C. F. R. (1989). Tracking algorithms using log-polar mapped image coordinates. *SPIE Proceedings on Intelligent Robots and Computer Vision VIII*, 1192.